Journal of Advanced Ceramics
2021, **10**(4): 758–767
https://doi.org/10.1007/s40145-021-0470-5
ISSN 2226-4108
CN 10-1154/TQ

Research Article

Enhanced mechanical property and tunable dielectric property of SiC_f/SiC–SiBCN composites by CVI combined with PIP

Chaokun SONG[a], Yongsheng LIU[a], Fang YE[a,*], Laifei CHENG[a,*], Pengfei ZHANG[b], Nan CHAI[c]

[a]*Science and Technology on Thermostructure Composite Materials Laboratory, Northwestern Polytechnical University, Xi'an 710072, China*
[b]*Beijing Spacecrafts, Beijing 100000, China*
[c]*Institut für Materialwissenschaft, Technische Universität Darmstadt, Darmstadt D-64287, Germany*

Received: November 29, 2020; Revised: February 24, 2021; Accepted: March 5, 2021

Abstract: The SiBCN matrix via chemical vapor infiltration (CVI) or/and polymer infiltration pyrolysis (PIP) technologies was orderly introduced to SiC_f/SiC composites to optimize the mechanical property and electromagnetic (EM) shielding effectiveness simultaneously. The BN interface with the thickness of 350 nm was designed to obtain a little stronger interface bonding. The flexural strength of SiC_f/SiC–SiBCN composites reached 545.45±29.59 MPa thanks to the crack deflection between the CVI SiC and CVI SiBCN, as well as CVI SiBCN and PIP SiBCN matrix because of the modulus difference between them. The fracture toughness (K_{IC}) with the value of 16.02±0.94 MPa·$m^{1/2}$ was obtained owing to the extension of crack propagation path. The adverse effect of stronger interface bonding was eliminated by the design of matrix microstructure for SiC_f/SiC–SiBCN composites. The thermal conductivity in the thickness direction was 7.64 W·(m·K)$^{-1}$ at 1200 ℃ and the electric resistivity decreased to 1.53×10^3 Ω·m. The tunable dielectric property was obtained with the coordination of wave-absorption CVI SiBCN matrix and impedance matching PIP SiBCN matrix, and the total shielding effectiveness (SE_T) attained 30.01 dB. It indicates that the SiC_f/SiC–SiBCN composites have great potential to be applied as structural and functional materials.

Keywords: SiC_f/SiC–SiBCN composites; chemical vapor infiltration (CVI); polymer infiltration pyrolysis (PIP); mechanical property; electromagnetic characteristic

1 Introduction

SiC_f/SiC composites have been widely investigated as a significant thermo-structural material in aero-engine and fusion reactor structural application because of the excellent characteristics (e.g., the low density, high specific modulus and strength, high toughness, oxidation resistance, etc.) [1,2]. Nevertheless, the matrix microcracks, resulting from the nonlinear mechanical characteristic when the SiC_f/SiC is loaded, as the diffusion channels of oxidizing medium markedly decrease the service life [3]. The SiBC matrix acting as self-healing component was introduced to SiC_f/SiC composites. With the formation of glass phase, the

* Corresponding authors.
E-mail: F. Ye, yefang511@nwpu.edu.cn
L. Cheng, chenglf@nwpu.edu.cn

SiC_f/SiC–SiBC composites exhibited outstanding mechanical property after exposing in air for 100 h at 800–1200 ℃ [4]. Above 1200 ℃, the self-healing ability of SiBC is insufficient because of its poor thermal stability and the sealing rate [5]. Another self-healing component with excellent thermal stability and self-healing performance is urgently needed.

SiBCN ceramic has low density (1.8 g/cm^3), small thermal expansion coefficient, good oxidation resistance (suitable for applying in air up to 1500 ℃), high temperature resistance (suitable for applying in inert environment up to 1800 ℃) [6], and outstanding creep resistance property [7], which has attracted extensive attention. The good thermal stability makes it widely used in thermal-structure unit and three aspects remain to be studied. Firstly, the mechanical property of SiBCN matrix modified SiC_f/SiC composites may be different from that of SiC_f/SiC composites resulting from the modulus difference between SiBCN and SiC. Secondly, the SiBCN matrix via chemical vapor infiltration (CVI) process shows continuous and dense morphology, and the dielectric property is tunable by controlling the deposition parameters [8,9]. The SiBCN matrix via pyrolysis (PIP) technology exhibits porous microstructure with some randomly distributed microcracks (owing to the volume shrinkage during the transformation from organic polymer to inorganic ceramic), and the permittivity is low with insulation characteristic [10–12]. The excellent electromagnetic (EM) shielding effectiveness, based on the matrix composition design using wave-absorbing CVI SiBCN and wave-transmitting PIP SiBCN, may be achieved. The impedance matching PIP SiBCN should be located externally to ensure the entry of electromagnetic wave (EMW) and the wave-absorbing chemical vapor infiltration (CVI) SiBCN should be introduced internally to attenuate the EMW. The SiBCN matrix should be orderly inserted into SiC_f/SiC via CVI and PIP technologies. Thirdly, the borosilicate or SiO_2 glass generates in virtue of the oxidation of SiBCN at high temperatures and oxidizing atmorsphere [13–15]. The self-healing performance can be obtained via viscous flow of borosilicate glass or SiO_2, and the service life of SiBCN matrix modified SiC_f/SiC composites can be prolonged [16]. The SiC_f/SiC–SiBCN composites are expected to be used in structural and functional integration area.

In this contribution, the SiC_f/SiC–SiBCN composites with different relative contents of CVI SiBCN and PIP SiBCN matrix were fabricated. The 350 nm-BN interface was chosen to obtain a little stronger bonding between fiber and matrix. The crack deflection was designed to occur at the interface between different matrices in addition to BN interface to extend oxygen diffusion path at matrix. The time for oxygen diffusion from matrix to BN interface and fiber would be prolonged. The BN interface and SiC fiber can be protected from corrosion and the duration of SiC_f/SiC–SiBCN composites is greatly increased. The microstructure and phase composition were carefully investigated. The electrical resistivity and thermal conductivity were measured. The flexural strength and K_{IC} at room temperature were tested, and the failure and toughness mechanism were discussed. The differences of mechanical behavior between SiC_f/SiC and SiC_f/SiC–SiBCN composites were presented. The *S*-parameter was further obtained in X-band and the EM shielding effectiveness was calculated.

2 Experimental

2.1 Raw materials

The near-stoichiometry SiC fiber (SiC_f) [17] was purchased from Xiamen University, China. The content of O is 0.42 wt% and the atomic ratio of C/Si is about 1.05. Each bundle contains 500 filaments. The diameter is about 12.5 μm and the tensile modulus is 341.85 GPa. The polyborosilazane [18] (PSNB, Institute of Chemistry, Chinese Academy of Sciences, China) was used as the polymer precursor.

2.2 Experimental procedure

The two-dimensional plain weave SiC fiber cloth was stacked and clamped with porous graphite moulds. The BN interface and SiC matrix were orderly deposited in SiC_f preform [19]. The semi-densified SiC_f/SiC composites with the density of 2.0 g/cm^3 were obtained. Then, SiC_f/SiC–SiBCN composites were acquired with the introduction of SiBCN matrix into semi-densified SiC_f/SiC composites. The CVI process was firstly chosen to fill the residual small pores between SiC_f bundles, and the big holes between the layers were finally divided into small holes by PIP technology. The SiBCN was deposited in semi-densified SiC_f/SiC via $SiCl_3CH_3$–BCl_3–NH_3–H_2–Ar system at 950 ℃. The fluxes of inlet gases were selected as follows: $[BCl_3]$:$[NH_3]$:[Ar]:[MTS]:$[H_2]$ = 0.96:0.79:8.21:1:10. Then, the PSNB was infiltrated into porous composites

Table 1 Intrinsic parameters of as-fabricated SiC_f/SiC–SiBCN composites

Sample	Label	Open porosity (%)	Density ($g \cdot cm^{-3}$)	Content of CVI SiC (vol%)	Content of CVI SiBCN (vol%)	Content of PIP SiBCN (vol%)
SiC_f/SiC	SiC_f/SiC	5.6	2.58	52.4	—	—
	1#	8.15	2.49	26.85	6	17
SiC_f/SiC–SiBCN	2#	8.42	2.46	26.58	15	8
	3#	9.4	2.39	26.6	22	—

at vacuum atmorsphere. The cross-linking process was finished at 170 ℃ for 2 h at N_2 atmorsphere, and the inorganic transition was completed at 1000 ℃ for 2 h at N_2 atmorsphere. The composition of obtained SiBCN has been shown in our previous work [15]. The relative content of CVI and PIP SiBCN was controlled by the cyclic number of CVI and PIP processes. The SiC_f/SiC composites were also manufactured to act as a control group. The volume fraction of SiC fiber in all composites was about 42%, and the intrinsic properties of as-fabricated SiC_f/SiC–SiBCN composites are shown in Table 1.

2. 3 Characterization

The open porosity and density were measured by Archimedes method. The morphology was observed by the scanning electron microscope (SEM, S4700; Hitachi, Japan). The phase composition was tested by the X-ray diffraction (XRD, Rigaku-D/max-2400; Tokyo, Japan) using Cu Kα (λ = 1.54 Å) radiation. The laser flash method (LFA 427, NETZSCH, Germany) was employed to measure the thermal diffusion (α) and heat capacity (C_p). The thermal conductivity (λ) can be calculated by the following equation: $\lambda = \alpha C_p \rho$, where ρ is the density of sample. The high resistance meter (4339B, Agilent, USA) was conducted to measure the direct-current electrical resistance. The electric resistivity was calculated based on the electrical resistance and dimension of composites. The *S*-parameters were obtained by the vector network analyzer (VNA, MS4644A, Anritsu, Japan) at 8.2–12.4 GHz (X-band), and the relative complex permittivity ε_r ($\varepsilon_r = \varepsilon' - j\varepsilon''$ where ε' and ε'' are the real and imaginary part of permittivity, respectively.) at 10 GHz was also acquired. The load–displacement curves were obtained by the three-point bending test with a loading speed of 0.5 mm/min using three 40 mm×5 mm×3 mm test bars. The K_{IC} was evaluated by single-edge notched beam (SENB) test with the loading speed of 0.05 mm/min using three 40 mm×3 mm×5 mm test bars. The modulus of fiber and matrices for SiC_f/SiC–SiBCN composites was measured by the nano indentation instrument (Hysitron, TI980, USA), and the maximum load used for nano indentation test is 10 mN. The loading and unloading curve (load with respect to displacement) can be obtained, and the modulus can be calculated based on the unloading curve. The moduli of fiber and matrix for SiC/SiC–SiBCN composites are shown in Table 2.

3 Results and discussion

3. 1 Microstructure and phase composition of SiC_f/SiC–SiBCN composites

The cross-section morphologies of as-fabricated SiC_f/SiC and SiC_f/SiC–SiBCN composites are shown in Fig. 1. The thickness of BN interface was about 350 nm (Fig. 1(a)), which maybe a little thinner comparing with conventional BN interface thickness (500 nm) in SiC_f/SiC composites [20] and would be unfavourable for mechanical properties. The dense CVI SiC matrix can be observed, and the small pores in fiber bundles were filled by SiC. The CVI and PIP

Table 2 Moduli of fiber and matrix for SiC/SiC–SiBCN composites

Testing position	SiC fiber	CVI SiC	CVI SiBCN	PIP SiBCN
Modulus (GPa)	325±9	418±20	76±13	150±6

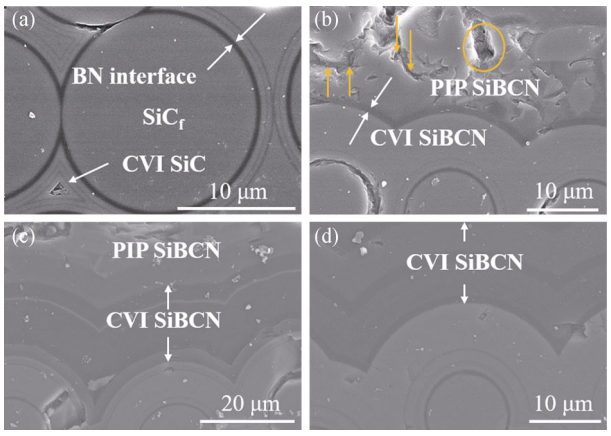

Fig. 1 Cross-section morphologies of SiC_f/SiC–SiBCN composites: (a) SiC_f/SiC, (b) 1#, (c) 2#, and (d) 3#.

SiBCN matrix were mainly located at inter-bundle region. The layered CVI SiBCN deposited via cyclic CVI technology was inserted outside SiC matrix (Figs. 1(b)–1(d)). The porous PIP SiBCN with some microcracks (the orange arrow shown in Fig. 1(b)) and pores (the orange circle shown in Fig. 1(b)) was finally introduced into SiC_f preform (Figs. 1(b) and 1(c)). When the SiC_f/SiC–SiBCN composites are loaded at high temperatures and oxidizing atmorsphere, the outer SiBCN matrix would be firstly oxidized with massive volume expansion and the borosilicate or SiO_2 glass generates according to previous studies [15,16,21]. The cracks can be quickly filled by above glass phase. The inner interphase and fiber would be protected from oxidation. The phase composition of as-fabricated composites is shown in Fig. 2. The characteristic diffraction peaks at 35.59°, 59.98°, 71.78°, and 75.49°, respectively, corresponding to (111), (220), (311), and (222) crystal planes of β-SiC can be observed. The CVI and PIP SiBCN were amorphous according to our previous work [22], and therefore no other diffraction peaks appeared in XRD patterns.

3. 2 Mechanical property and fracture mechanism

The flexural load–displacement curves are shown in Fig. 3. The flexural strength of SiC_f/SiC was 325.46±69.78 MPa. As for SiC_f/SiC–SiBCN composites, the flexural strength of 1#, 2#, and 3# was 445.69±36.76 MPa, 545.45±29.59 MPa, and 420.75±47.38 MPa, respectively. The curves contained linear and non-linear segments before the stress reached the maximum. Then the curves of both SiC_f/SiC and SiC_f/SiC–SiBCN composites suddenly declined after the curves passed its peak. The fracture morphologies are exhibited in Fig. 4. The fracture of both SiC_f/SiC and SiC_f/SiC–SiBCN composites

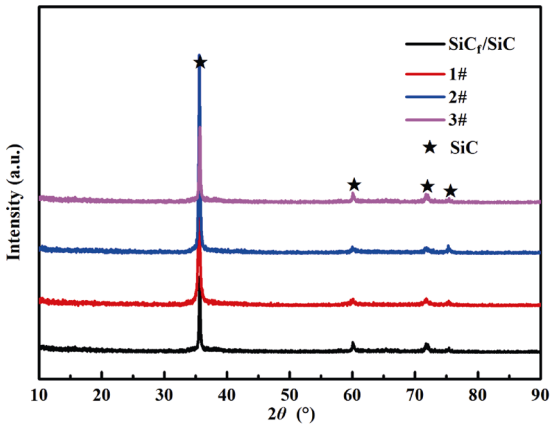

Fig. 2 XRD patterns of as-fabricated composites.

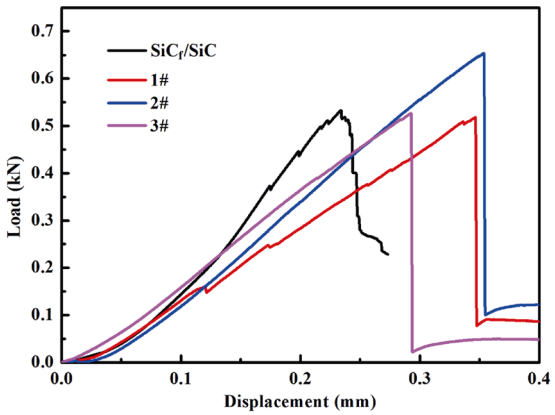

Fig. 3 Three-point bending test load–displacement curves of as-fabricated composites.

was flat (Figs. 4(a)–4(d)). The interface debonding and fiber pullout with a few micrometers in length can be observed in all composites (Figs. 4(e)–4(h)). The crack deflection at matrix appeared, and the crack propagation path was prolonged (Figs. 4(e)–4(h)). The delamination cracking (Figs. 4(i)–4(l)) was related to the layered matrix structure [23], and the crack propagation energy was consumed. The toughness can be further enhanced.

As the composites are loaded, the elastic deformation firstly occurs. With the increase of load, the matrix cracks appear [13,24]. As for SiC_f/SiC, the cracks quickly extend in SiC matrix. The sufficient crack deflection at interface area is limited resulting from the strong interface bonding. The fibers quickly rupture and the samples fail. The load–displacment curve suddenly drops. In SiC_f/SiC–SiBCN composites, the SiBCN matrix firstly cracks owing to higher strains (originating from the lower modulus according to Table 2). The crack deflection occurs at porous and cracked PIP SiBCN matrix, also at layered CVI SiBCN matrix according to our previous studies [22], which relieves the stress concentration at a crack tip. The crack deflection exists at the interface between PIP and CVI SiBCN matrix (Fig. 5(a)), also at the region between CVI SiBCN and CVI SiC matrix (Figs. 5(b)–5(d)) owing to the modulus difference between them. With the load further improving, the cracks density in SiBCN matrix is saturated, and the SiC matrix begins to play the role of undertaking load at higher stress. The matrix cracks in SiC rapidly initiate and propagate. The interface debonding also occurs in some BN interface regions. Finally, fibers fracture at the top of load–displacement curves, and the composites fail. The conditions for interface debonding are similar according to He and Hutchinson [25] model with the same fiber

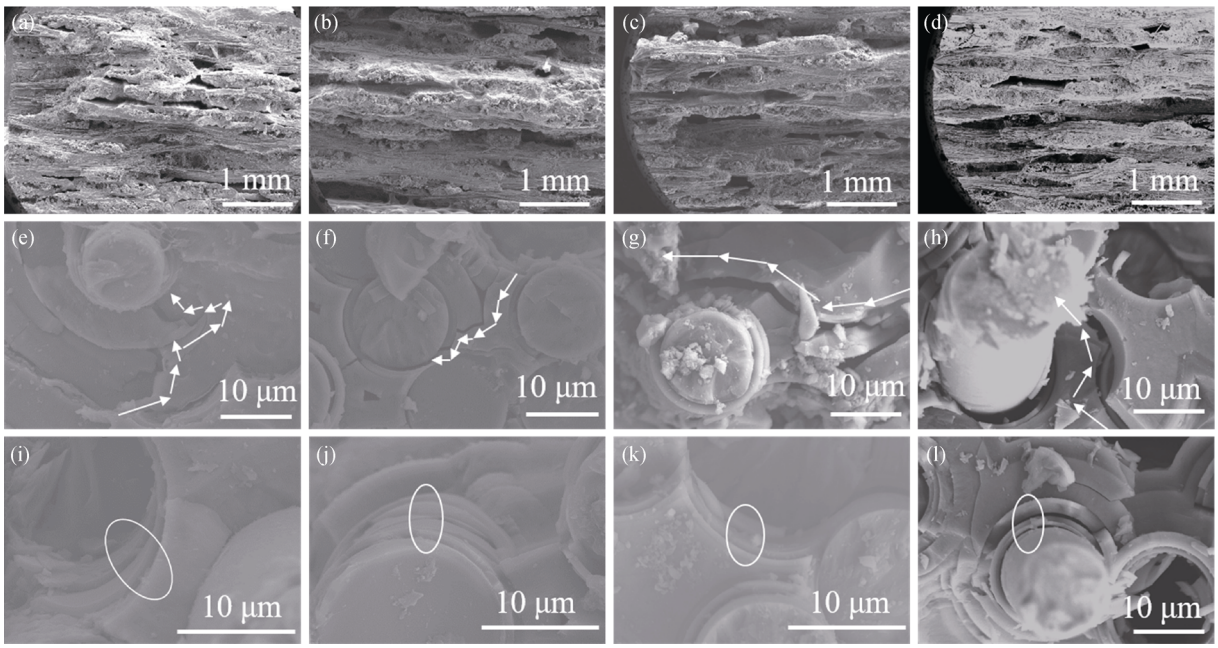

Fig. 4 Fracture morphologies of as-fabricated composites after three-point bending test: (a, e, and i) SiC_f/SiC, (b, f, and j) 1#, (c, g, and k) 2#, and (d, h, and l) 3#.

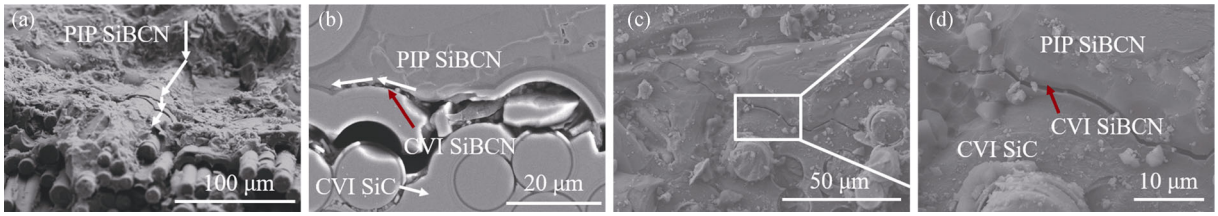

Fig. 5 Crack deflection in multiphase matrix: (a, b) 1#, (c) 2#; (d) the area in the box of (c) ((a, c, and d) are fresh fractures, and (b) is originating from the polished sample at the center area of 1# after three-point bending test).

volume fraction, BN interface thickness and CVI SiC matrix around BN interface for all composites. The interface debonding situation and fiber pullout length are similar for SiC_f/SiC and SiC_f/SiC–SiBCN composites according to Fig. 4. The difference between SiC_f/SiC and SiC_f/SiC–SiBCN composites is the load transfer process in multiphase matrix. The crack deflection, occuring in PIP SiBCN, layered CVI SiBCN matrix, also at the interface between PIP and CVI SiBCN matrix, CVI SiBCN and CVI SiC matrix, significantly prolongs the crack propagation path. The flexural strength of SiC_f/SiC–SiBCN composites is further improved comparing with SiC_f/SiC composites resulting from the crack deflection at the interface of different matrices with different moduli. When the SiC_f/SiC–SiBCN composites work at high temperatures and oxidizing environment, the cracks in matrix can be quickly healed by glass phase generating from the oxidation of SiBCN matrix, and the crack deflection further extends the oxygen diffusion path. With the reasonable design of interface and matrix, the BN interface and SiC fiber can be avoided to degenerate by increasing the crack deflection in matrix.

The load–displacement curves obtained by fracture toughness test are shown in Fig. 6. The fracture toughness (K_{IC}) of SiC_f/SiC, 1#, 2#, and 3# was 6.21±2.88, 13.24±0.63, 16.02±0.94, and 12.29±0.96 $MPa \cdot m^{1/2}$, respectively. The crack propagation route is shown in Fig. 7. In SiC_f/SiC composites, the crack deflection was hardly observed and the crack propagation path was almost straight resulting from the strong bonding [26] between fiber and matrix with 350 nm-BN interface (Fig. 7(a)). With regard to SiC_f/SiC–SiBCN composites, the fracture toughness was significantly enhanced as a result of the prolonging of crack propagation path (Figs. 7(b)–7(d)). The crack deflection occurred at the interface between PIP SiBCN and CVI SiBCN matrix, as well as between SiC and SiBCN. The

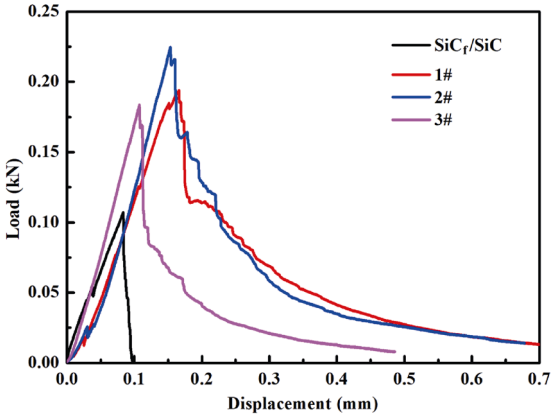

Fig. 6 Fracture toughness test load–displacement curves of as-fabricated composites.

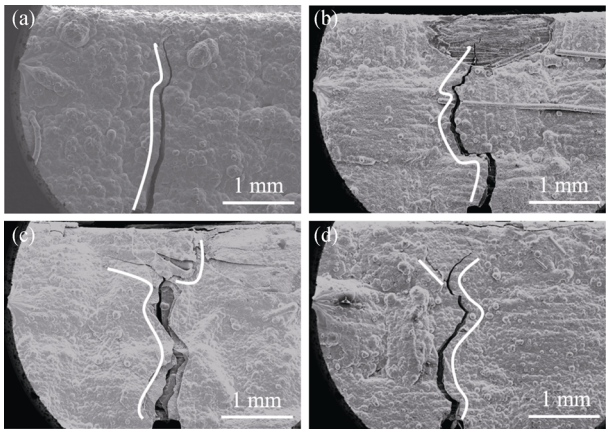

Fig. 7 Crack propagation path via fracture toughness test: (a) SiC_f/SiC, (b) 1#, (c) 2#, and (d) 3#.

crack diffusion energy was consumed and the toughness was improved. The SiC_f/SiC–SiBCN composites, possessing excellent flexural strength and fracture toughness, have great potential to be applied as thermo-structural materials.

3. 3 Physical and dielectric properties

The thermal conductivity in the thickness direction as a function of the temperature is shown in Fig. 8(a). The thermal conductivity of SiC_f/SiC was 8.89 $W\cdot(m\cdot K)^{-1}$ at 400 ℃. The thermal conductivity of SiC_f/SiC–SiBCN declined with the introduction of SiBCN matrix, which can be attributed to the low thermal conductivity of SiBCN ceramic (3 $W\cdot(m\cdot K)^{-1}$) [6] and the relatively high porosity of the modified composites (Table 1). Heat transfer mode contains radiation, convection, and conduction [27]. The thermal conduction is the main heat transfer mode in solid materials, corresponding to the transfer of a particle's vibrational energy (or a

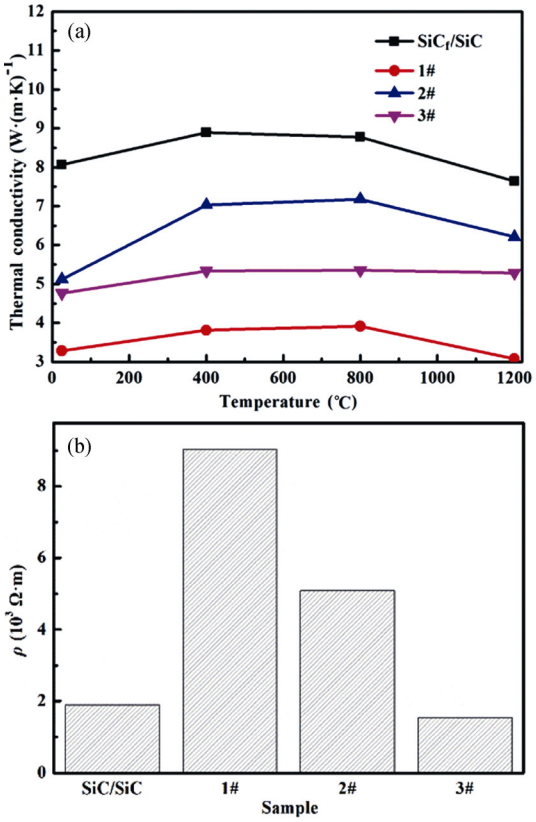

Fig. 8 (a) Thermal conductivity and (b) electric resistivity of as-fabricated composites.

phonon) to adjacent particles [28]. Hence, the crystallinity has a significant effect on thermal conductivity. The highly crystalline materials usually possess high thermal conductivity [29,30]. As for SiC_f/SiC–SiBCN composites, the amorphous SiBCN matrix significantly affected the thermal conductivity of composites. The thermal conductivity (λ) can be theoretically estimated by the Debye equation:

$$\lambda = \frac{C_p v l}{3} \tag{1}$$

where v is the average phonon velocity and l is the phonon free path. With the increase of temperature, the v is improved. Meanwhile, the lattice vabration is also intensified, and the l is correspondingly decreased. As for SiC_f/SiC, the increase of v was dominant comparing with the decline of l from 25 to 400 ℃. The vabriation tendency of thermal conductivity from 25 to 400 ℃ is different from the work by Feng *et al*. [31,32], which may be ascribed to different stacked ways of SiC fibric, volume fraction of SiC fiber, and interface phase. Then the variation of l had a more significant effect on λ at 400–1200 ℃. The maximum value of λ was 8.89 $W\cdot(m\cdot K)^{-1}$ when the temperature was 400 ℃, and

then it decreased to 7.64 $W\cdot(m\cdot K)^{-1}$ at 1200 ℃. After the introduction of SiBCN ceramic, the rise of v controlled the λ from 25 to 600 ℃. Then, the λ began to decrease with the reduction of l at 600–1200 ℃. The maximum value of λ was 3.92, 7.18, and 5.35 $W\cdot(m\cdot K)^{-1}$ at 600 ℃, corresponding to 1#, 2#, and 3#, respectively. According to the results of Zhang *et al*. [18], the atomic rearrangement occurs when the temperature is above preparation temperature of SiBCN. Some by-product gases generate and the volume shrinks. It means the porosity of composites may increase. This condition has harmful effect on thermal conductivity when the temperature is above 1000 ℃. The electric resistance at room temperature was also measured and the electric resistivity is shown in Fig. 8(b). The value of electric resistivity for SiC_f/SiC was 1.9×10^3 Ω·m [19]. As for 1#, the value of electric resistivity was 9.04×10^3 Ω·m because the electric resistivity of PIP SiBCN matrix was high. With the increase of CVI SiBCN matrix, the electric resistivity decreased, which can be attributed to the abundant free carbon phase in CVI SiBCN [22]. The electric resistivity of 2# and 3# was 5.09×10^3 and 1.53×10^3 Ω·m, respectively.

The dielectric property is estimated by the relative complex permittivity, and the tunable dielectric property of as-fabricated SiC_f/SiC–SiBCN is shown in Table 3. The value of ε' was 41.68, 27.71, 34.06, and 50.55, and the ε'' was 31.64, 37.57, 42.3, and 46.91 at 10 GHz for SiC_f/SiC, 1#, 2#, and 3#, respectively. The loss tangent ($\tan\delta = \varepsilon''/\varepsilon'$) was 0.759, 1.355, 1.242, and 0.928, respectively. The intrinsic permittivity of SiBCN matrix was also tested and shown in Table 3. The ε' and ε'' of PIP SiBCN were 4.92 and 0.0863 at 10 GHz, respectively. The low ε'' means poor EMW absorbing characteristic and good impendace matching ability of PIP SiBCN matrix. In order to obtain the permittivity of CVI SiBCN, the Si_3N_4 substrate with the wave-transparent characteristic was placed into the CVI furnace. According to the deposition processing of SiC_f/SiC–SiBCN composites, the SiBCN was deposited on Si_3N_4 substrate. The ε' and ε'' of Si_3N_4 were 4.42 and 0.000863 at 10 GHz, respectively. The ε' and ε'' of Si_3N_4–SiBCN composite ceramics with about 8 vol% of CVI SiBCN were 4.50 and 0.219 at 10 GHz, respectively. It indicated the introduction of SiBCN and the formation of interface polarization [33] at the Si_3N_4/SiBCN interface area significantly enhanced the dielectric property. The ε' and ε'' of CVI SiBCN were 22.52 and 13.67 calculated according to the rule of mixtures [34]. The CVI SiBCN with high permittivity (thanks to its abandant free carbon) had excellent EMW attenuation property comparing with that of PIP SiBCN. The 1#, with higher content of PIP SiBCN matrix, possessed the lowest ε' and ε'' in SiC_f/SiC–SiBCN composites. With the increase of CVI SiBCN content, the value of permittivity rised. The ε' and ε'' of 2# increased 0.229 times and 0.126 times comparing with that of 1#, respectively. The ε' and ε'' of 3# increased 0.824 times and 0.249 times comparing with that of 1#, respectively. The increment of ε'' was lower than that of ε', and the $\tan\delta$ of 2# and 3# correspondingly reduced. Additionally, the heterogeneous interface, SiC/SiBCN (CVI), and SiBCN (CVI)/SiBCN (PIP), formed with the introduction of SiBCN matrix. The polarization phenomenon was enhanced owing to the dielectric property difference between different matrices in the external alternating electromagnetic fields [35].

Table 3 Dielectric property of as-fabricated composites at 10 GHz

Sample	ε'	ε''	$\tan\delta$
SiC_f/SiC	41.68	31.64	0.759
1#	27.71	37.57	1.355
2#	34.06	42.30	1.242
3#	50.55	46.91	0.928
PIP SiBCN	4.92	0.0863	0.0175
Si_3N_4	4.42	0.000863	0.000195
Si_3N_4–SiBCN	4.50	0.219	0.0487
CVI SiBCN*	22.52	13.37	0.607

* represents the theoretical permittivity of CVI SiBCN calculated according to the rule of mixtures.

The EM shielding effectiveness was calculated using scattering parameters (*S*-parameters: S_{11}, S_{12}, S_{21}, and S_{22}), which was obtained by VNA. The SE_T consists of reflection shielding effectiveness (SE_R), absorption shielding effectiveness (SE_A), and multiple reflection shielding effectiveness (SE_M). When the SE_T > 15 dB, the SE_M can be ignored. The SE_T is described as follows:

$$SE_T = SE_R + SE_A \tag{2}$$

where SE_R and SE_A can be calculated using the reflection coefficient (R) and the transmission coefficient (T) by the following equations:

$$SE_R = -10\log(1-R) \tag{3}$$

$$SE_A = -10\log[T/(1-R)] \tag{4}$$

where R and T can be expressed by the following equations [36,37]:

$$R = |S_{11}|^2 = |S_{22}|^2 \quad (5)$$

$$T = |S_{12}|^2 = |S_{21}|^2 \quad (6)$$

The calculated shielding effectiveness is shown in Fig. 9. The SE_T of SiC_f/SiC, 1#, 2#, and 3# was 23.82, 26.08, 26.23, and 30.01 dB at 10 GHz, respectively. The SE_R of SiC_f/SiC, 1#, 2#, and 3# was 8.46, 6.58, 7.23, and 7.86 dB, respectively. The corresponding SE_A was 15.36, 19.50, 19.00, and 22.15 dB, respectively. The SE_A was remarkably greater than SE_R, and it

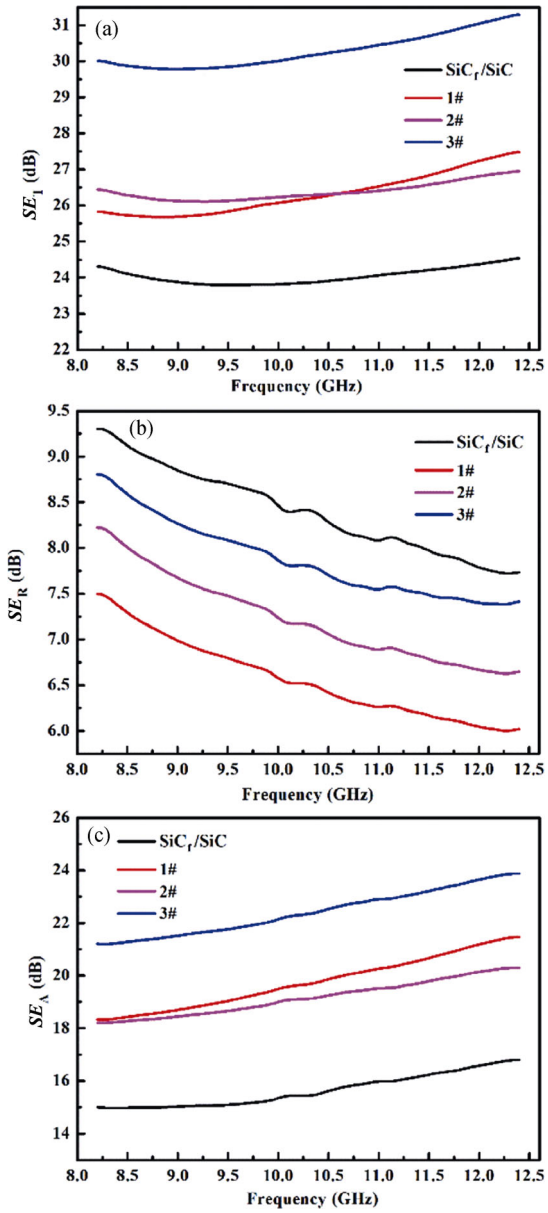

Fig. 9 Shielding effectiveness of as-fabricated composites: (a) SE_T, (b) SE_R, and (c) SE_A.

indicated that the EM shielding property of both SiC_f/SiC and SiC_f/SiC–SiBCN composites was mainly dependent on EMW absorption. It is worthy noting that the EM shielding effectiveness of 3#, with the value of 30.01, was the best among the modified composites. With the introduction of impedance-matched PIP SiBCN matrix, the SE_R of SiC_f/SiC–SiBCN composites decreased comparing with that of SiC_f/SiC. It meant less EMW was reflected on the surface of samples and more EMW entered the composites. With the enhanced dielectric property of SiC_f/SiC–SiBCN composites, the SE_R gradually improved. The R and absorption coefficient (A) at 10 GHz were calculated to further analyze the EM properties of composites. For 1#, 2#, and 3#, the value of R was 0.78, 0.81, and 0.84, and the value of A was 0.22, 0.19, and 0.16, respectively. The R of 3# is the highest and the A is the lowest. It indicated that more and more EMW was reflected when it reached the surface of as-fabricated composites resulting from the huge differences between air and as-fabricated composites with increased CVI SiBCN. Deriving from the effective attenuation of EMW at the interface between the successive layers of CVI SiBCN matrix, the 3# had the highest value of SE_A among the SiC_f/SiC–SiBCN composites [22]. The SiC_f/SiC–SiBCN composites, with tunable dielectric and EM shielding effectiveness, can act as outstanding EM shielding materials.

4 Conclusions

The SiC_f/SiC–SiBCN composites were successfully prepared via CVI combined with PIP technologies. The following conclusions can be summarized:

1) The stronger interface bonding with the thickness of BN interface about 350 nm was designed, and the internal pores of the fiber bundles were filled by CVI SiC matrix. The amorphous CVI SiBCN and PIP SiBCN matrix were orderly introduced outside the SiC matrix.

2) The flexural strength and fracture toughness of SiC_f/SiC–SiBCN composites, containing 15 vol% CVI SiBCN matrix and 8 vol% PIP SiBCN matrix, were 545.45±29.59 MPa and 16.02±0.94 MPa·$m^{1/2}$, respectively. The crack propagation path was further increased in the layered CVI SiBCN matrix and cracked PIP SiBCN matrix, additionally at the interface area between CVI and PIP SiBCN matrix, CVI SiBCN and SiC matrix. The crack propagation energy was severely

attenuated, and enhanced mechanical properties can be obtained comparing with SiC_f/SiC composites.

3) Resulting from the higher open porosity and the introduction of amorphous SiBCN matrix with low thermal conductivity, the thermal conductivity of SiC_f/SiC–SiBCN composites in the thickness direction was lower than SiC_f/SiC composites. Owing to the abundant free carbon in CVI SiBCN, the electrical resistivity decreased with the increased content of CVI SiBCN matrix.

4) The EM shielding property of SiC_f/SiC–SiBCN composites was mainly dependent on SE_A. The SE_T, SE_R, and SE_A of 3# were 30.01, 7.86, and 22.15 dB, respectively, which shows that the SiC_f/SiC–SiBCN composites are the excellent candidate to act as structural and functional composites.

Acknowledgements

This work was supported by the National Natural Science Foundation of China (Grant Nos. 52072304, 51632007, and 51872229), the 111 Project of China (B08040), and the National Science and Technology Major Project (Grant No. 2017-VI-0007-0077).

References

[1] Igawa N, Taguchi T, Nozawa T, *et al*. Fabrication of SiC fiber reinforced SiC composite by chemical vapor infiltration for excellent mechanical properties. *J Phys Chem Solids* 2005, **66**: 551–554.

[2] Lamouroux F, Bertrand S, Pailler R, *et al*. Oxidation-resistant carbon-fiber-reinforced ceramic-matrix composites. *Compos Sci Technol* 1999, **59**: 1073–1085.

[3] Naslain RR. SiC-matrix composites: Nonbrittle ceramics for thermo-structural application. *Int J Appl Ceram Technol* 2005, **2**: 75–84.

[4] Sun XN, Yin XW, Fan XM, *et al*. Oxidation resistance of SiC/SiC composites containing SiBC matrix fabricated by liquid silicon infiltration. *J Eur Ceram Soc* 2017, **38**: 479–485.

[5] Liu YS, Wan JJ, Zuo XZ, *et al*. Oxidation behavior of 2D C/SiC composites coated with multi-layer SiC/Si–B–C/SiC coatings under wet oxygen atmosphere. *Appl Surf Sci* 2015, **353**: 214–223.

[6] Baldus P, Jansen M, Sporn D. Ceramic fibers for matrix composites in high-temperature engine applications. *Science* 1999, **285**: 699–703.

[7] Riedel R, Ruswisch LM, An L, *et al*. Amorphous silicoboron carbonitride ceramic with very high viscosity at temperatures above 1500 ℃. *J Am Ceram Soc* 2010, **81**: 3341–3344.

[8] Liu YS, Chai N, Liu XF, *et al*. The microstructure and dielectric properties of SiBCN ceramics fabricated via LPCVD/CVI. *J Am Ceram Soc* 2015, **98**: 2703–2706.

[9] Zhao MX, Liu YS, Chai N, *et al*. Effect of SiBCN content on the dielectric and EMW absorbing properties of SiBCN–Si_3N_4 composite ceramics. *J Eur Ceram Soc* 2018, **38**: 1334–1340.

[10] Ye F, Zhang LT, Yin XW, *et al*. Dielectric and EMW absorbing properties of PDCs–SiBCN annealed at different temperatures. *J Eur Ceram Soc* 2013, **33**: 1469–1477.

[11] Ye F, Zhang LT, Yin XW, *et al*. Dielectric and microwave-absorption properties of SiC nanoparticle/SiBCN composite ceramics. *J Eur Ceram Soc* 2014, **34**: 205–215.

[12] Zhang YJ, Yin XW, Ye F, *et al*. Effects of multi-walled carbon nanotubes on the crystallization behavior of PDCs–SiBCN and their improved dielectric and EM absorbing properties. *J Eur Ceram Soc* 2014, **34**: 1053–1061.

[13] Lu B, Yue Z. Oxidation behavior of SiC–SiBCN ceramics. *Ceram Int* 2015, **41**: 1023–1030.

[14] Cinibulk MK, Parthasarathy TA. Characterization of oxidized polymer-derived SiBCN fibers. *J Am Ceram Soc* 2010, **84**: 2197–2202.

[15] Song CK, Ye F, Liu YS, *et al*. Microstructure and dielectric property evolution of self-healing PDC–SiBCN in static air. *J Alloys Compd* 2019, **811**: 151584.

[16] Tan X, Liu W, Cao LM, *et al*. Oxidation behavior of a 2DSiC_f/BN/SiBCN composite at 1350–1650 ℃ in air. *Mater Corros* 2018, **69**: 1227–1236.

[17] Chen LF, Zhang, L, Cai ZH, *et al*., Effects of oxidation curing and sintering additives on the formation of polymer-derived near-stoichiometric silicon carbide fibers. *J Am Ceram Soc* 2010, **91**: 428–436.

[18] Zhang ZB, Zeng F, Han JJ, *et al*. Synthesis and characterization of a new liquid polymer precursor for Si–B–C–N ceramics. *J Mater Sci* 2011, **46**: 5940–5947.

[19] Ma XK, Yin XW, Cao XY, *et al*. Effect of heat treatment on the mechanical properties of SiC_f/BN/SiC fabricated by CVI. *Ceram Int* 2016, **42**: 3652–3658.

[20] Information on https://ntrs.nasa.gov/citations/20050217198.

[21] Wang CH, Liu YS, Zhao MX, *et al*. Effects of upgrading temperature on electromagnetic shielding properties of three-dimensional graphene/SiBCN/SiC ceramic composites. *Ceram Int* 2019, **45**: 21278–21285.

[22] Song CK, Liu XF, Ye F, *et al*. Mechanical and Dielectric Properties of SiC_f/BN/SiBCN composites via different synthesis technologies. *J Eur Ceram Soc* 2019, **39**: 4417–4423.

[23] Naslain R. The concept of layered interphases in SiC/SiC. *Ceram Trans* 1995, **58**: 23–39.

[24] Ding Q, Ni DW, Wang Z, *et al*. Mechanical properties and microstructure evolution of 3D C_f/SiBCN composites at elevated temperatures. *J Am Ceram Soc* 2018, **101**: 4699–4707.

[25] He MY, Hutchinson JW. Crack deflection at an interface between dissimilar elastic materials. *Int J Solids Struct* 1989, **25**: 1053–1067.
[26] Cao XY, Yin XW, Fan XM, *et al*. Effect of PyC interphase thickness on mechanical behaviors of SiBC matrix modified C/SiC composites fabricated by reactive melt infiltration. *Carbon* 2014, **77**: 886–895.
[27] Lee JH, Lee SH, Choi C, *et al*. A Review of thermal conductivity data, mechanisms and models for nanofluids. *Int J Micro-Nano Scale Transp* 2011, **1**: 269–322.
[28] Burger N, Laachachi A, Ferriol M, *et al*. Review of thermal conductivity in composites: mechanisms, parameters and theory. *Prog Polym Sci* 2016, **61**: 1–28.
[29] Monje IE, Louis E, Molina JM. Optimizing thermal conductivity in gas-pressure infiltrated aluminum/diamond composites by precise processing control. *Compos Part A-Appl S* 2013, **48**: 9–14.
[30] Toberer ES, Baranowski LL, Dames C. Advances in Thermal Conductivity. *Annu Rev Mater Res* 2012, **42**: 179–209.
[31] Feng W, Zhang LT, Liu YS, *et al*. Fabrication of SiC_f–CNTs/SiC composites with high thermal conductivity by vacuum filtration combined with CVI. *Mat Sci Eng A-Struct* 2016, **662**: 506–510.
[32] Feng W, Zhang LT, Liu YS, *et al*. Increasing the thermal conductivity of 2D SiC/SiC composites by heat-treatment. *Fusion Eng Des* 2015, **90**: 110–118.
[33] Shao YQ, Lu WB, Chen H, *et al*. Flexible ultra-thin Fe_3O_4/MnO_2 core-shell decorated CNT composite with enhanced electromagnetic wave absorption performance. *Compos Part B-Eng* 2018, **144**: 111–117.
[34] Penn SJ, Alford NM, Templeton A, *et al*. Effect of porosity and grain size on the microwave dielectric properties of sintered alumina. *J Am Ceram Soc* 1997, **80**: 1885–1888.
[35] Quan B, Liang XH, Ji GB, *et al*. Dielectric polarization in electromagnetic wave absorption: Review and perspective. *J Alloys Compd* 2017, **728**: 1065–1075.
[36] Nicolson AM, Ross GF. Measurement of the intrinsic properties of materials by time-domain techniques. *IEEE Trans Instrum Meas* 1970, **19**: 377–382.
[37] Weir WB. Automatic measurement of complex dielectric constant and permeability at microwave frequencies. *Proc IEEE* 1974, **62**: 33–36.